

Lattice generalization of the Dirac equation to general spin and the role of the flat bandBalázs Dóra,^{1,*} Janik Kailasvuori,^{2,3} and R. Moessner²¹*Department of Physics, Budapest University of Technology and Economics, Budafoki út 8, HU-1111 Budapest, Hungary*²*Max-Planck-Institut für Physik komplexer Systeme, Nöthnitzer Str. 38, DE-01187 Dresden, Germany*³*International Institute of Physics, Universidade Federal do Rio Grande do Norte, 59078-400 Natal-RN, Brazil*

(Received 14 April 2011; revised manuscript received 3 October 2011; published 7 November 2011)

We provide a setup for generalizing the two-dimensional pseudospin $S = 1/2$ Dirac equation, arising in graphene's honeycomb lattice, to general pseudospin S . We engineer these band structures as a nearest-neighbor hopping Hamiltonian involving stacked triangular lattices. We obtain multilayered low-energy excitations around half-filling described by a two-dimensional Dirac equation of the form $H = v_F \mathbf{S} \cdot \mathbf{p}$, where \mathbf{S} represents an arbitrary spin S (integer or half-integer). For integer S , a flat band appears, the presence of which modifies qualitatively the response of the system. Among physical observables, the density of states, the optical conductivity, and the peculiarities of Klein tunneling are investigated. We also study Chern numbers as well as the zero-energy Landau-level degeneracy. By changing the stacking pattern, the topological properties are altered significantly, with no obvious analog in multilayer graphene stacks.

DOI: [10.1103/PhysRevB.84.195422](https://doi.org/10.1103/PhysRevB.84.195422)

PACS number(s): 05.30.Fk, 81.05.ue, 71.10.Fd, 73.21.Ac

I. INTRODUCTION

Since the seminal work on monolayer graphene (a single sheet of carbon atoms forming a honeycomb lattice) in 2004,¹ a lot of attention has been focused on this material. Its low-energy properties close to half-filling (i.e., pristine graphene) are well described by a two-dimensional massless Dirac equation, with the speed of light replaced by the appropriate Fermi velocity $\sim 10^6$ m/s. Most of the unusual electronic properties of this material can be traced back to the massless Dirac nature of its quasiparticles and their unusual Berry phase. These include its linearly vanishing density of states (DOS) around half-filling, resembling a d -wave superconductor, unusual Landau quantization in a perpendicular magnetic field, and the anomalous half-integer quantum Hall effect. Additionally, phenomena such as the universal optical conductivity and high optical transparency Klein tunneling through electric barriers are also distinguishing features.

The appearance of the massless Dirac equation has triggered further research to find out whether other systems can possess similar behavior or even generalizations of the $S = 1/2$ Dirac physics to, e.g., higher dimensions, including additional terms. In the context of ultracold atom in optical lattices, several proposals have been put forward to realize a generalization of graphene physics in terms of the $S = 1$ Dirac equation.²⁻⁵ Generalizations to higher S with spin-dependent hoppings⁶ as well as with artificial magnetic field⁷ are also possible.

Here, we present a family of lattices, the low-energy excitations around given fillings of which are described by a generalized two-dimensional Dirac equation

$$H = v_F \mathbf{S} \cdot \mathbf{p}, \quad (1)$$

where $\mathbf{p} = (p_x, p_y, 0)$, and $\mathbf{S} = (S_x, S_y, S_z)$ is the matrix representation of an arbitrary spin S (integer or half-integer), and v_F is the Fermi velocity. These lattices consist of stackings of triangular layers, and include slabs of face-centered-cubic and hexagonal close-packed lattices as special cases. Technically, the notion Weyl Hamiltonian⁶ is more appropriate for Eq. (1) for $S > 1/2$, although we refer to it as generalized Dirac

equation (sometimes omitting the "generalized") since our motivation comes primarily from graphene and its pseudospin- $1/2$ Dirac equation.

Our model is characterized by considerable simplicity and tunability. Furthermore, it contains a unique feature, absent from previous lattice realizations of higher spin- S Hamiltonians: the possibility of (through a simple lateral shift in the layer positions) changing the chiral properties of individual interlayer hoppings, without changing the spectrum. However, there are considerable changes on other properties, for example, topological properties such as the multiplicity of the zero-energy Landau level degeneracy in magnetic field.

The paper is organized as follows. In Sec. II, we introduce the lattice and discuss some of its general features. We then proceed to analyze the properties resulting from such a band structure: density of states (Sec. III), optical conductivity (Sec. IV), Chern numbers and spin Chern numbers of the band structure (Sec. V), zero-mode degeneracy in both a uniform as well as a nonuniform magnetic field (Sec. VI), and Klein tunneling (Sec. VII) for the spin-1 case, focusing on tunneling into the flat band. We also derive the general matching condition for the wave function for arbitrary pseudospin S . Finally, the relevant symmetry properties are highlighted in an Appendix.

The $S = 1/2$ version is realized in graphene⁸ and on the surface of three-dimensional (3d) topological insulators.⁹ Of the recent proposals for the $S = 1$ case,²⁻⁵ our construction includes the dice lattice. Our work in many respects is complementary to Ref. 6, where diverse properties (topology, transport) of the spin- S Dirac equation were studied using a different lattice realization with spin-dependent hoppings.

II. BAND-STRUCTURE ENGINEERING

To set the stage, let us first cast the analysis of graphene's honeycomb lattice in a form that lends itself to generalization. The bipartite honeycomb lattice has two atoms (A and B) per unit cell; each sublattice forms a triangular lattice and the

hopping Hamiltonian in Fourier space takes the form

$$H = \begin{bmatrix} 0 & tf(\mathbf{k}) \\ tf^*(\mathbf{k}) & 0 \end{bmatrix}, \quad (2)$$

where t is the hopping amplitude and a the intercarbon distance, while $f(\mathbf{k}) = 1 + 2 \exp(i3k_y a/2) \cos(\sqrt{3}k_x a/2)$.

At half-filling, the Fermi surface consists of two inequivalent Dirac points K and K' at momenta $\pm(2\pi/3\sqrt{3}a, 2\pi/3a) = \mathbf{k}_\pm$, respectively. Expanding around these points leads to two copies of the two-dimensional Dirac equation for $S = 1/2$, with the sublattice providing the (pseudo)spin degree of freedom:

$$S_x = \frac{1}{2} \begin{pmatrix} 0 & 1 \\ 1 & 0 \end{pmatrix}, \quad S_y = \frac{1}{2} \begin{pmatrix} 0 & -i \\ i & 0 \end{pmatrix}. \quad (3)$$

$v_F = 3ta$, the missing factor $1/2$ as opposed to graphene⁸ arising since the eigenvalues of the spin are $\pm 1/2$.

If we now think of the honeycomb lattice as a layered structure, with the A and B triangular sublattices offset in height by an amount h , it is natural to ask what happens if one adds a third, and then further, triangular layers (see Fig. 1). For small h , the nearest neighbors of a given site are in the layers directly above and below. When the layers are stacked in the sequence of the face-centered-cubic lattice in a $[111]$ direction, one obtains a band diagonal hopping Hamiltonian for a system of $2S + 1$ layers:

$$H_S = t \begin{bmatrix} 0 & \alpha_{01} f(\mathbf{k}) & 0 & & 0 \\ \alpha_{01}^* f^*(\mathbf{k}) & 0 & \alpha_{12} f(\mathbf{k}) & & 0 \\ 0 & \alpha_{12}^* f^*(\mathbf{k}) & 0 & \ddots & \alpha_{2S-1,2S} f(\mathbf{k}) \\ & 0 & \ddots & \ddots & 0 \\ & & 0 & \alpha_{2S-1,2S}^* f^*(\mathbf{k}) & 0 \end{bmatrix}, \quad (4)$$

where we have allowed for different interlayer hopping strengths by introducing the α 's. Indeed, regardless of the choice of $\alpha_{i,i+1}$, several properties of the spectrum of H_S immediately follow from the form of its characteristic polynomial $C_S(\lambda, \mathbf{k}) = \det(H_S - \lambda \mathbb{1})$, which reads as

$$C_S(\lambda, \mathbf{k}) = |tf(\mathbf{k})|^{2S+1} \det(\alpha^+ + \alpha^- - \tilde{\lambda} \mathbb{1}), \quad (5)$$

where $\tilde{\lambda} = \lambda/|f(\mathbf{k})|$ is independent of \mathbf{k} , and so is $\alpha_{ij}^+ = (\alpha_{ji}^-)^* = \alpha_{i,i+1} \delta_{j,i+1}$. First, near the Dirac points (K and K'), all bands are linearly dispersing simply because $|f(\mathbf{k})| \propto |\mathbf{k} - \mathbf{k}_\pm|$. Second, for integer S , the Hamiltonian must display a flat band. The matrix $\alpha^+ + \alpha^-$ possesses a symmetric spectrum (if $\tilde{\lambda}$ is an eigenvalue, then so is also $-\tilde{\lambda}$). The Hamiltonian also possesses this symmetry, which can be phrased as a chiral symmetry $\Sigma H(\mathbf{k}) \Sigma^\dagger = -H(\mathbf{k})$ with Σ a unitary operator, as further discussed in the Appendix. For an odd number $2S + 1$ of bands, the chiral symmetry implies that (at least) one eigenvalue $\tilde{\lambda}$ must be zero, which translates into a flat band $\lambda = |f(k)|\tilde{\lambda} = 0$.¹⁰

If now, in addition, we choose the interplane hopping amplitudes so that $\alpha^+ = S^+$, where $S^+ = S_x + iS_y$ is the raising operator for spin S , we obtain a spectrum $E_n(\mathbf{k}) = nt|f(\mathbf{k})|$, where $n = -S, -S + 1, \dots, S$. This requires placing the adjacent layers at certain distances from each other, so that the

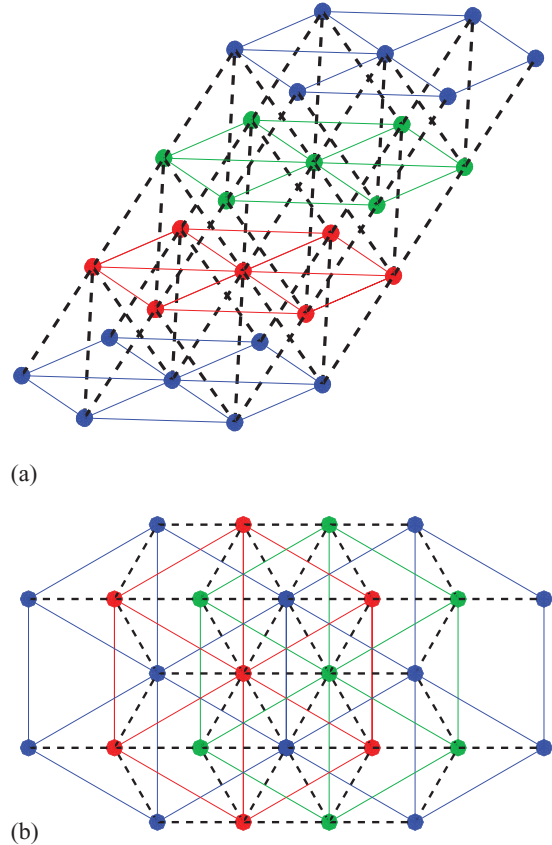


FIG. 1. (Color online) The schematic representation of the family of lattice models leading to the spin- S Dirac equation is shown from the side (a) and from above (b). The dashed lines denote interlayer hopping processes, while the intralayer thin solid lines are guides to the eye, emphasizing the planar triangular structure, but do not represent any hoppings. The lowest and highest A planes (blue) are exactly on top of each other. For $S = 1/2$, only two adjacent layers need to be considered (e.g., the red A, and green B layers), for $S = 1$, three neighboring ABC layers (e.g., lower blue, red, and green), for $S = 3/2$, all four layers, while for higher S 's, one needs to continue upward or downward with ABCABC... stackings. Note that the interlayer hoppings should be unequal to realize the perfect Dirac equation [Eq. (8)].

overlap of the wave functions would produce the appropriate hopping integrals between subsequent layers, the relative strength of which is further specified in Eq. (9).

As a result, we obtain an effective Hamiltonian near the K point

$$H_S(\mathbf{p}) = v_F \mathbf{S} \cdot \mathbf{p}. \quad (6)$$

Here, $\mathbf{p} = \mathbf{k} - \mathbf{k}_+$ measures the (small) distance from the Dirac point at K , and similarly for the K' point. If we finally add a potential of strength ΔS_z , which can, in principle, be generated straightforwardly via an electric field applied perpendicular to the layers, representing distinct chemical potentials for each layer, we have

$$E_n(\mathbf{p}) = n \sqrt{v_F^2 (p_x^2 + p_y^2) + \Delta^2}. \quad (7)$$

For integer S , $n = 0$ invariably corresponds to a flat band, however, no longer due to chiral symmetry but due to a less

general symmetry that is specific to the low-energy Dirac-type Hamiltonians and that requires fine tuning of the parameters α_{ij} . Fortunately for experimental realizations, rather natural setups such as equidistant layers will satisfy the conditions for a flat band, as discussed in the Appendix in more detail.

It can now be verified straightforwardly that the cases $S = 1/2$ and 1 correspond to the known instances of the honeycomb and dice (or T_3) lattices,^{2,8} respectively. The $S = 3/2$ case for four layers reads as

$$H = \begin{bmatrix} 0 & \sqrt{3}tf(\mathbf{k}) & 0 & 0 \\ \sqrt{3}tf^*(\mathbf{k}) & 0 & 2tf(\mathbf{k}) & 0 \\ 0 & 2tf^*(\mathbf{k}) & 0 & \sqrt{3}tf(\mathbf{k}) \\ 0 & 0 & \sqrt{3}tf^*(\mathbf{k}) & 0 \end{bmatrix}, \quad (8)$$

which can be supplemented with an additional gap, coming from ΔS_z with $S_z = \text{diag}(3/2, 1/2, -1/2, -3/2)$. A very similar lattice structure has been proposed in Ref. 11.

Note that the simple form of the Hamiltonian also gives immediate access to the wave functions in layer (pseudospin) space, as its eigenfunctions are obtained from a simple rotation in spin space: the quantization axis of \mathbf{S} is given by an effective field direction \mathbf{h} , the components of which are given by $\text{Re}f(\mathbf{k})$, $\text{Im}f(\mathbf{k})$, and Δ , respectively. The various α prefactors above and below the diagonal are chosen according to the conventional matrix representation of the spin matrices.¹² For example, above the diagonal, the matrix elements of the raising ladder operator appear as

$$\langle n' | S^+ | n \rangle = \delta_{n',n+1} \sqrt{S(S+1) - n(n+1)}, \quad (9)$$

where $S_z |n\rangle = n|n\rangle$. The resulting spectrum consists of equidistant energy levels at each given momentum. As mentioned above, with a different choice of α , the spectrum would still be linear. The Dirac cones are robust in this sense. Furthermore, although the bands at a given momentum would not necessarily be equidistant anymore, the flat band will still survive if certain symmetries are present, as discussed in the Appendix.

For $\Delta = 0$, the wave function corresponding to the flat band is such that the probability of finding a particle in even layers is exactly zero. For example, in an $S = 1$ trilayer, the red plane, sandwiched between the blue and green ones (see Fig. 1), is completely blocked for the flat-band wave function.

The stacking we propose here is of course quite familiar. A succession of triangular planes ABCABC. . . , as displayed in Fig. 1, is just the face-centered-cubic lattice viewed along a [111] direction. Another stacking, ABABA. . . , corresponds to the hexagonal close-packed lattice structure. The hopping Hamiltonian [Eq. (4)] is simply modified to take into account this stacking: $f(\mathbf{k})$ is replaced by its complex conjugate for hopping BA, CB, or AC. For example, the stacking ABCB would result in

$$H_S = t \begin{bmatrix} 0 & \alpha_{01}f(\mathbf{k}) & 0 & 0 \\ \alpha_{01}^*f^*(\mathbf{k}) & 0 & \alpha_{12}f(\mathbf{k}) & 0 \\ 0 & \alpha_{12}^*f^*(\mathbf{k}) & 0 & \alpha_{23}^*f^*(\mathbf{k}) \\ 0 & 0 & \alpha_{23}f(\mathbf{k}) & 0 \end{bmatrix}. \quad (10)$$

We will say that the chirality between the third and the fourth layers has been flipped.

The spectrum (and, in particular, Dirac cones and flat bands) is not affected by this change, which affects only the phase of the matrix elements. Indeed, a unitary transformation, changing the i th spinor entry $\psi_i(k) \rightarrow \exp[2i \arg f(k)]\psi_i(k)$, changes $f^*(k) \rightarrow f(k)$ in $H_{S,i-1,i}$.

Around half-filling, where the continuum description applies, this corresponds to flipping the chirality in the Hamiltonian between adjacent layers. This change of chirality is at the origin of a change in the Berry curvature (detailed in Sec. V). Note that one can successively “fix” the phases of the off-diagonal terms to agree with a reference stacking without altering diagonal terms that may be present.

Finally, we emphasize again that, for a layer separation $h < \tilde{a}\sqrt{2/3}$, where \tilde{a} is the triangular lattice constant, our Eq. (4) represents nearest-neighbor hoppings only. Having outlined a path toward general lattices with Dirac physics, we next discuss some of the basic properties of such electronic systems.

III. DENSITY OF STATES

The density of states (DOS) for $\Delta = 0$ is given, using the low-energy Dirac Hamiltonians, by

$$\rho(\omega) = \sum_{\mathbf{p}, n=-S}^S \delta[\omega - E_n(\mathbf{p})] = \frac{A_c |\omega|}{2\pi v_F^2} \sum_{n>0} \frac{1}{n^2} + \delta(\omega)\delta_{S,\text{integer}} \quad (11)$$

per spin, valley, and unit cell, with A_c being the unit-cell area. The DOS remains linear in energy, similar to graphene, but exhibits a sharp peak due to the flat band^{2,13} for integer-spin realizations. The DOS can be simplified to

$$\rho(\omega) = \frac{A_c |\omega|}{2\pi v_F^2} \left(\frac{\pi^2}{6} - \Psi'(S+1) \right) + \delta(\omega) \quad (12)$$

for integer spins, and

$$\rho(\omega) = \frac{A_c |\omega|}{2\pi v_F^2} \left(\frac{\pi^2}{2} - \Psi'(S+1) \right) \quad (13)$$

for half-integer spins, where $\Psi(x)$ is Euler’s digamma function. Due to the momentum integral in Eq. (11), these results are only valid for $|k| \ll k_c$ with k_c the cutoff, which translates to $|\omega| \ll v_F k_c$. Note that, for large spin $S \gg 1$, the maximal slope of the DOS right at the Fermi energy is $\pi^2/8$ times larger than for spin-1/2 for half-integer spins, and $\pi^2/6$ times larger than for spin-1 for integer spins. The S dependence of the slope of the DOS is shown in Fig. 2, which changes very little with S in the integer or half-integer sector. With increasing S , additional Dirac cones appear with increasing slope, thus, with a much reduced contribution to the DOS. As opposed to that, these high-energy bands contribute more at high energies, since their bandwidth also increases with S .

The original lattice model provides us with additional features not captured by the low-energy approximation, such as the presence of van Hove singularities around $\omega = nt$ with $n = -S, -S+1 \dots S$ but $n \neq 0$ as $\rho(\omega) \sim \ln(\omega/|nt|)$. In addition to the two peaks for graphene with $S = 1/2$, an increasing number of additional pairs of peaks appear in the DOS for $S > 1$.

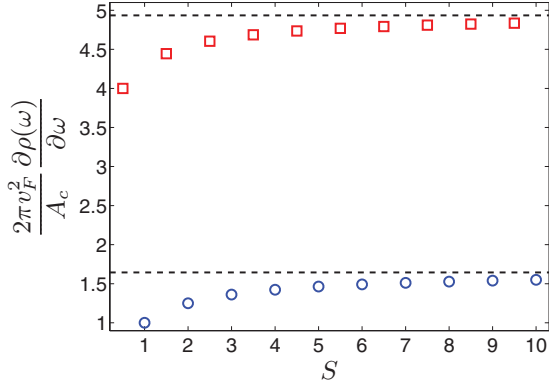


FIG. 2. (Color online) The slope of the linear in energy density of states is plotted for various values of S ; the dashed black lines denote the asymptotic values $\pi^2/6$ and $\pi^2/2$ for integer and half-integer spins, respectively.

IV. OPTICAL CONDUCTIVITY

Another characteristic quantity of Dirac fermions is the optical conductivity, which, for $S = 1/2$ at half-filling and $T = 0$, is completely structureless and constant. In the presence of additional Dirac bands, new interband transitions occur. The current operator in the x directions is given by $j_x = v_F S_x$. Its equation of motion as well as those of the other spin components are

$$\partial_t S_x = v_F p_y S_z, \quad (14)$$

$$\partial_t S_y = -v_F p_x S_z, \quad (15)$$

$$\partial_t S_z = v_F (p_x S_y - p_y S_x) \quad (16)$$

for a given momentum. This is easily solved for $S_x(t)$ as

$$S_x(t) = S_x [\sin^2(\varphi_p) \cos(v_F p t) + \cos^2(\varphi_p)] + \frac{1}{2} S_y \sin(2\varphi_p) \times [1 - \cos(v_F p t)] + S_z \sin(\varphi_p) \sin(v_F p t), \quad (17)$$

where $\tan(\varphi_p) = p_x/p_y$.

The current-current correlation function is evaluated from this as

$$\begin{aligned} \chi_{JJ}(t) &= \sum_{n, \mathbf{p}} \langle S_x(t) S_x - S_x S_x(t) \rangle \\ &= 2i \sum_{n, \mathbf{p}} \langle S_y \rangle \sin(\varphi_p) \sin(v_F p t) \\ &= 2i \sum_{n, \mathbf{p}} n p \sin^2(\varphi_p) \sin(v_F p t). \end{aligned} \quad (18)$$

After Fourier transformation, the optical conductivity contains two parts as

$$\sigma(\omega) = D \delta(\omega) + \sigma_{\text{inter}}(\omega) \quad (19)$$

per electron spin and valley, and the Drude weight is

$$D = \frac{e^2 \pi T}{h} [S + 1/2] \ln \left[2 \cosh \left(\frac{\mu}{2k_B T} \right) \right], \quad (20)$$

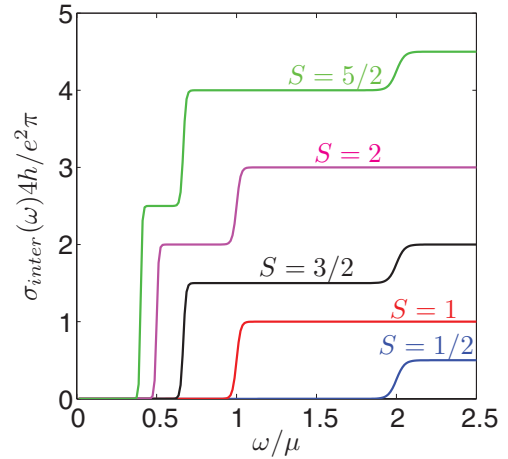


FIG. 3. (Color online) The interband part of the optical conductivity for the spin- S Dirac equation is shown for $k_B T/\mu = 0.0125$ for several values of S . The number of possible interband transitions is $\lfloor S + 1/2 \rfloor$.

which agrees with that of graphene¹⁴ for $S = 1/2$, while the interband part reads as

$$\sigma_{\text{inter}}(\omega) = -\frac{e^2 \pi}{4h} \sum_{n=-S}^S n f(n\hbar\omega), \quad (21)$$

where $f(x) = 1/\{\exp[(x - \mu)/k_B T] + 1\}$ is the Fermi function, μ the chemical potential, and $\lfloor x \rfloor$ denotes the integer part. Since the particles residing on the flat band can not propagate, their group velocity is zero, so that their contribution vanishes to the Drude weight. This explains the integer part function. On the other hand, they have a finite matrix element between adjacent levels, and contribute to interband transport, which contains all allowed $2S$ processes between $2S + 1$ levels.

At the Dirac point ($\mu = 0$) at $T = 0$, the Drude weight disappears, and the interband conductivity reads as

$$\sigma_{\text{inter}}(\omega) = \frac{e^2 \pi}{4h} \left(\frac{S(S+1)}{2} + \begin{cases} \frac{1}{8} & \text{half-integer } S \\ 0 & \text{integer } S \end{cases} \right). \quad (22)$$

Away from the Dirac point, $\lfloor S + 1/2 \rfloor$ interband transitions are allowed, as can be checked in Figs. 3 and 4.

The calculated intraband and interband optical conductivities differ significantly from those in graphene. First, the interband part is sensitive to the number of bands and away from half-filling, several steps are possible as opposed to graphene, where only a single step is allowed. Second, the universal value for the optical conductivity at half-filling and finite frequencies is proportional to pseudospin- S value, which should also affect the transparency as

$$\begin{aligned} \mathcal{T} &= \left(1 + \frac{2\pi}{c} \sigma(\omega) \right)^{-2} \\ &\approx 1 - \pi \alpha_{\text{QED}} \left[S(S+1) + \begin{cases} \frac{1}{4} & \text{half-integer } S \\ 0 & \text{integer } S \end{cases} \right], \end{aligned} \quad (23)$$

where the lower line is obtained upon Taylor expanding the upper line, and is only valid for $S \lesssim 2$. Here, valley and physical spin degeneracies are included, $\alpha_{\text{QED}} = e^2/\hbar c$

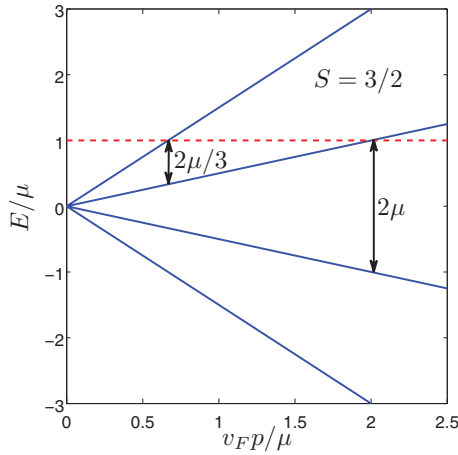


FIG. 4. (Color online) The band structure of $S = 3/2$, visualizing the minimal frequency of the allowed optical transition. As opposed to graphene, transitions well below $\omega = 2\mu$ are possible.

is the fine-structure constant, and c the speed of light. For $S = 1/2$, this reproduces the $\mathcal{T} \simeq 97.7\%$ optical transparency of graphene. Therefore, the universal value of the optical response immediately reveals the underlying pseudospin- S structure, as shown in Fig. 5. Third, while the interband response takes the contribution of the flat band into account, the intraband one (Drude) is insensitive to its presence due to the zero group velocity of the flat band.

V. TOPOLOGICAL PROPERTIES OF THE BAND STRUCTURE

Here, we discuss the topological properties of our model in the absence of a gauge field. It will turn out that there can be topologically nontrivial ground states. The topological invariant we study, i.e., the spin Chern number, depends on the number of layers and on the band fillings. However, it does not appear to depend on the stacking configuration, although the Berry curvature, from which it is calculated, does.

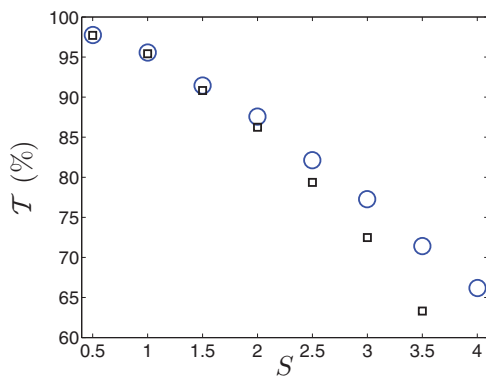


FIG. 5. (Color online) The universal optical transparency is shown for half-filling as a function of S . The blue circles denote the exact expression from Eq. (23) (upper line), while the black squares show the approximate formula, valid for small S [lower line in Eq. (23)].

We study the integral of the Berry curvature, where the contribution to the Berry curvature from a given band is given by

$$\mathcal{B}_n = \sum_{\substack{n = -S, \\ n' \neq n}}^S \frac{2 \operatorname{Im}[\langle n, \mathbf{k} | \partial_{k_x} H | n', \mathbf{k} \rangle \langle n', \mathbf{k} | \partial_{k_y} H | n, \mathbf{k} \rangle]}{[E_n(\mathbf{k}) - E_{n'}(\mathbf{k})]^2}, \quad (24)$$

where n is a band index and $|n, \mathbf{k}\rangle$ a single-particle eigenstate of H with eigenvalue $E_n(\mathbf{k})$. In the thermodynamic limit, the summation over momentum turns into an integral. When this integral goes over a compact manifold such as the Brillouin zone (BZ), one obtains a topological invariant called the first Chern number

$$C_n = \int_{\text{BZ}} \frac{d^2 k}{2\pi} \mathcal{B}_n. \quad (25)$$

A nonzero Chern number requires breaking of time-reversal symmetry (TRS). This can be accomplished by an external magnetic field as in the integer quantum Hall effect,¹⁵ but also by gap terms that break TRS.¹⁶ Settings of the latter kind with flat bands with nonzero Chern number have been reported.¹⁷⁻¹⁹ In this section, we only study gap terms that preserve TRS, hence, the Chern number is zero. However, the Chern number is integrated from a nontrivial Berry curvature that derives mainly from the two singularities in the Brillouin zone: the Dirac cones at the K and K' points. When calculating the total vorticity of a configuration of quantized vortices, it is usually enough to calculate the vorticity of the individual vortices as if they were isolated, and then add up the quanta (including the sign) to obtain the total vorticity. Similarly, it is usually enough to calculate the integral of the Berry curvature for individual Dirac cones, living not on a Brillouin zone, but on the infinite plane of momenta and then add up their contributions to obtain the same result, which would originate from integrating the full band structure over the Brillouin zone. We will use both approaches and demonstrate explicitly (in Table I) that they match.

TABLE I. The integral of the Berry curvature for a single pseudospin- S Dirac cone (C_n^K) and the spin-dependent Chern number (C_n^\uparrow) for the lattice model are shown for all possible, nonequivalent stacking patterns for $S < 5/2$ and $\Delta > 0$. These are evaluated numerically for both the continuum and lattice models, and their relation can be checked using Eq. (33). Note that $C_n^\uparrow = -C_n^\downarrow$.

S	Stacking	C_n^K (single cone)	C_n^\uparrow (lattice)
1/2	AB	(1/2, -1/2)	(1, -1)
1	ABC	(1, 0, -1)	(2, 0, -2)
1	ABA	(1/2, -1, 1/2)	(0, 0, 0)
3/2	ABCA	(3/2, 1/2, -1/2, -3/2)	(3, 1, -1, -3)
3/2	ABAB	(1/2, -1/2, 1/2, -1/2)	(1, -1, 1, -1)
3/2	ABCB	(5/4, -1/4, -5/4, 1/4)	(1, 1, -1, -1)
2	ABCAB	(2, 1, 0, -1, -2)	(4, 2, 0, -2, -4)
2	ABCAC	(15/8, 1/2, -3/4, -3/2, -1/8)	(2, 2, 0, -2, -2)
2	ABCBC	(11/8, 0, -3/4, 0, -5/8)	(2, 0, 0, 0, -2)
2	ABCBA	(5/4, -1/2, -3/2, -1/2, 5/4)	(0, 0, 0, 0, 0)
2	ABABA	(1/2, -1/2, 0, -1/2, 1/2)	(0, 0, 0, 0, 0)
2	ABACA	(0, -1, 0, 1, 0)	(0, -2, 0, 2, 0)

Another topological invariant is the spin Chern number. It is calculated from the contributions to the Chern number individually for the two components of the physical spin, but instead of adding up the two contributions to get the Chern number, one takes the difference to obtain the spin Chern number.

The charge Chern number is related to a topologically quantized Hall current of charge¹⁵

$$\sigma_{xy} = \frac{e^2}{h} \sum_n C_n, \quad (26)$$

with the summation taken over filled bands. Likewise, the spin Chern number can be used to determine the quantized spin-Hall conductivity. This is the case with the intrinsic spin-orbit coupling (SOC) of graphene²⁰

$$H_{SO} = \Delta \tau_z S_z \sigma_z, \quad (27)$$

which preserves TRS. Here, τ_z and σ_z refer to the valley and physical spin degrees of freedom. We will generalize this SOC to arbitrary pseudospin S .

In addition, the different stacking configurations lead to interesting changes in the integral of the Berry curvature in the single-cone approximation, which calls for future research on the role of stacking order on topological properties.

A. Single pseudospin- S Dirac cone

Let us first focus on the integral of the Berry curvature of a single spin- S Dirac equation for spinless electrons. In itself, it is usually not a topological invariant, but the topological invariants can often be understood in terms of the contributions for the single cones, and the latter can, in the simplest case, be evaluated analytically. In some cases, these nonzero contributions add up to zero, as must be the case for the Chern number in the time-reversal symmetric setup that we consider. However, we will also see that, for the spin Chern number, another topological invariant, the contributions add up to an invariant that can be nonzero.

For a given band in the spin- S Dirac equation, assuming a gap of the form ΔS_z , the integral of the Berry curvature is evaluated around the K point by assuming an isolated Dirac cone in the momentum plane in the expression of Eq. (24). Thus,

$$C_n^K = \int_0^\infty \frac{n \Delta v_F^2 p dp}{[(v_F p)^2 + \Delta^2]^{3/2}} = n \text{sign}(\Delta), \quad (28)$$

where n takes the allowed values of S_z , which also indexes the bands. For the $S = \frac{1}{2}$ Dirac equation, this reproduces the known result²¹ $C_\pm = \pm \frac{1}{2} \text{sign}(\Delta)$ with the upper (lower) sign corresponding to the upper (lower) Dirac cone.

The contribution to the transverse conductivity from an individual cone at the Dirac point K is the sum of the above C_n^K 's from the filled bands. In the Dirac-cone approximation, a gap exists only around zero energy (between $n = -1/2$ and $1/2$ for half-integer spin or between the bands $n = -1, 0$, and 1 for integer spin). Therefore, as long as the chemical potential satisfies $|\mu| < \Delta/2$ for half-integer and $0 < |\mu| < |\Delta|$ for integer spins, one obtains also in the low-energy approximation

a half-integer quantized transverse response (per spin and valley)

$$\sigma_{xy}^K = \frac{e^2}{h} \sum_{n < 0} C_n^K = -\frac{e^2}{h} \frac{S(S+1)}{2} \text{sign}(\Delta) - \frac{e^2}{h} \begin{cases} 0 & \text{for integer } S, \\ \frac{\text{sign}(\Delta)}{8} & \text{for half-integer } S. \end{cases} \quad (29)$$

An increasing chemical potential will cut into some bands that destroy the half-integer quantization of σ_{xy}^K .

By choosing a stacking different from ABCAB... , other decompositions across the bands can be obtained for the Berry curvature in the single-cone approximation, which leads to a result different from Eq. (28). For example, for $S = 1$, i.e., the trilayer with ABC stacking, we obtain for positive Δ that $(C_1^K, C_0^K, C_{-1}^K) = (1, 0, -1)$ per spin and valley. By flipping the chirality between the second and third layers (which correspond to an ABA stacking), we obtain instead $(1/2, -1, 1/2)$ as integrals of the Berry curvature for the successive bands. (These integrals were evaluated numerically, in contrast to those related to the spin- S Hamiltonians.) Most importantly, the 0 contribution of the flat band gets modified to 1. Various stacking patterns, the variety of which grows with the number of layers, are listed in Table I. As we demonstrate next, the integral of the Berry curvature around a single cone can be used to determine the spin Chern number of the lattice model.

B. Chern numbers on the lattice

To obtain a topological invariant, the full Brillouin zone (including the K' point) has to be considered. For a setting with TRS, which we consider here, the Chern number has to be zero, even though the Berry curvature contributions around the individual cones may be nonzero, in which case they cancel. This cancellation can be avoided by involving the physical spin: by generalizing the intrinsic SOC of graphene in Eq. (27) to general spin- S , we can end up with nonzero *spin* Chern number and, thus, finite spin-Hall conductivity.

By going back to the original lattice model and defining the full lattice version of Eq. (27) following Ref. 22 as

$$H_{SO, \text{lattice}} = \frac{2\Delta}{3\sqrt{3}} \sigma_z S_z [2 \sin(\sqrt{3}k_x a/2) \cos(3k_y a/2) - \sin(\sqrt{3}k_x a)], \quad (30)$$

which should be added to Eq. (4), we get the spin Chern numbers C_n^s from Eq. (24) (with a numerical integration over the entire Brillouin zone) as

$$C_n^s = C_n^\uparrow - C_n^\downarrow = 4n \text{sign}(\Delta), \quad (31)$$

where the factor 4 comes from the valley and physical spin degrees of freedom, and C^σ is the Chern number for up ($\sigma = \uparrow$) or down ($\sigma = \downarrow$) spins and $C_n^\uparrow = -C_n^\downarrow$.

Whether the system qualifies as a spin-Hall insulator is decided²² by the Z_2 invariant ν , defined by $\nu = \sum_n C_n^s / 2 \pmod{2} = \sum_n 2n \text{sign} \Delta \pmod{2}$, and summation is taken over filled bands.

We thus find that integer pseudospins contribute with even numbers to the sum in ν , and are topologically trivial

for the lattices in Fig. 1, giving $\nu = 0$. By contrast, half-integer spins contribute with odd numbers to the sum, and having an even number of filled bands at half-filling (i.e., $S = 3/2, 7/2, 11/2, \dots$) adds up to an even number, thus, again $\nu = 0$. As opposed to this, half-integer spins with $S = 1/2, 5/2, 9/2, \dots$ have an odd number of filled bands at half-filling, adding up to an odd number, resulting in $\nu = 1$ and topologically nontrivial behavior.

The spin-dependent Chern numbers of the lattice model can be obtained from the single-cone results of the previous section. In the single-cone approximation, the spin-orbit coupling of Eq. (30) simplifies to Eq. (27). These single-cone contributions to the Chern number satisfy

$$C_n^K(\Delta) = -C_n^{K'}(\Delta) = C_{-n}^K(-\Delta) = -C_{-n}^{K'}(-\Delta). \quad (32)$$

The opposite sign of the gap term for the two Dirac points derives from τ_z in Eq. (27).

By taking both Dirac points into account, we obtain from the single-cone results the spin Chern number

$$C_n^\uparrow = C_n^K(\Delta) + C_n^{K'}(-\Delta) = C_n^K(\Delta) - C_{-n}^K(\Delta). \quad (33)$$

The result agrees with the result in Eq. (31) found from integrating over the Brillouin zone using the full band structure. Equation (33) immediately implies that the spin Chern number of the flat band is zero ($C_0^\uparrow = 0$), regardless of the value of $C_0^K(\Delta)$.

We can also consider other stacking patterns, as we did in the single-cone case. The correspondences in Eq. (33) hold for arbitrary stacking patterns on the lattice. For example, the trilayer with ABA stacking with $\Delta > 0$ yields zero-spin Chern numbers for all bands, unlike the $S = 1$ case derived from the ABC stacking. However, like the ABC stacking, the ABA gives a spin Chern number that is topologically trivial. Results for other stackings are shown in Table I. One interesting general conclusion that we can draw based on these results is that, while the single-cone Chern number contributions for each band are redistributed significantly with different stacking patterns, this does not affect the Z_2 topological invariant. This invariant will therefore be determined only by the number of layers, but not by the stacking. We have also checked that all nonequivalent stackings for the $S = 5/2$ case (not shown here) give $\nu = 1$ at half-filling. The invariance to changes in stacking applies also away from half-filling, as long as the chemical potential lies between the bands.

We can also engineer nearly flat bands with nontrivial topology, similarly to Refs. 17–19: when $\Delta \gg t$, all bands become practically flat as $E_n(p) \approx n\Delta + nt^2|f(\mathbf{k})|^2/2\Delta$, i.e. the hopping occurs only to second order in perturbation theory. Therefore, it becomes possible to fill the separate bands one by one. Then, for example, the quarter-filled $S = 3/2$ case, which corresponds to a completely filled $E_{-3/2}(p)$ band, becomes topologically nontrivial with $\nu = 1$ for all stackings. Note that, when $\Delta \ll t$, quarter-filling in this case gives partially filled $E_{-3/2}(p)$ and $E_{-1/2}(p)$ bands. In the same vein, the 1/3-filled $S = 5/2$ lattice with flattened bands ($\Delta \gg t$) is topologically trivial with $\nu = 0$. Thus, a trivial ground state can become nontrivial (and vice versa) when the chemical potential is lowered or increased to the next band gap.

Another observation we have made is that, while the topological invariants (the Chern number and the spin Chern number) are robust with respect to the variations of α 's in Eq. (4), the integrals of the Berry curvature for a single cone (C_n^K) are not invariant. However, for some stacking patterns, C_n^K is rather insensitive to changes in α 's. In particular, the single-cone results for ABABA and ABACA stackings are also recovered for uniform interlayer hoppings.

We close this section with the remark that topological invariants do not depend only on S , but also on the number of nonequivalent Dirac cones and, thus, on the specific form of the lattice. For example, T_3 and Lieb lattices^{23,24} with even and odd number of $S = 1$ cones, respectively, belong to different Z_2 class.⁹ In the presence of intrinsic SOC, the T_3 lattice with two inequivalent cones possesses the trivial Z_2 index. On the contrary, the Lieb lattice has a single cone in its band structure and has therefore a ground state with a nontrivial Z_2 invariant, and realizes a spin-Hall insulator in the presence of SOC.

VI. TOPOLOGICAL PROPERTIES IN THE PRESENCE OF A MAGNETIC FIELD

A topological property of our lattice that turns out to depend dramatically on the stacking configuration is the number of zero modes in a magnetic field. In the case of a uniform magnetic field, these zero modes are nothing but $E = 0$ Landau-level (LL) states. We now show that by changing the stacking from the ABCAB... stacking to some other stacking, the $E = 0$ Landau-level degeneracy will increase by a multiple.

This can immediately be seen in experiment as an increased step at $\mu = 0$ in the steps of quantized Hall conductivity σ_{xy} as a function of chemical potential, in a way analogous to the well-known examples of monolayer and bilayer graphene: in the former, all Landau levels have the same degeneracy, while in the latter, the degeneracy of the $E = 0$ LL is twice that of the others.^{25,26} Such degeneracies and their lifting play an important role, for example, at integer fillings in the context of multicomponent quantum Hall ferromagnetism (see, e.g., Ref. 27).

The reason for this increased multiplicity thanks to restacking is rather easy to understand. Consider the gauge-invariant momentum operator $\mathcal{D}_i(\mathbf{x}) = -i\partial_{x_i} - A_i(\mathbf{x})$. The existence of zero modes relies on the fact that one of the chiral Dirac operators $\mathcal{D}_\pm = -i(\partial_x \pm i\partial_y) - (A_x \pm iA_y)$ has a nontrivial kernel when the net flux of \mathbf{A} is bigger than one flux quantum. The number of states in the kernel is given by the number of flux quanta. Depending on the sign of the total flux, one finds nontrivial solutions either to $\mathcal{D}_+\psi = 0$ or to $\mathcal{D}_-\psi = 0$, but not to both. This latter fact comes into play in an interesting way when we start to flip the chiralities of the hoppings between individual layers by restacking, as we will now come to.

As in graphene, we discuss the Landau-level spectrum in the linearized regime of the low-energy Hamiltonians, that is, in terms of the Dirac cones. (In the case of the full band structure, we can not write the Hamiltonian only in terms of the chiral combinations \mathcal{D}_\pm , which are necessary for the analytical discussion of zero modes.) The Dirac Hamiltonian is then written in real space and the magnetic field is introduced

by minimal coupling. For the ABCA stacking, we find, at the Dirac point K ,

$$H_{ABCA} = \begin{bmatrix} 0 & \alpha_{01}\mathcal{D}_- & 0 & 0 \\ \alpha_{01}^*\mathcal{D}_+ & 0 & \alpha_{12}\mathcal{D}_- & 0 \\ 0 & \alpha_{12}^*\mathcal{D}_+ & 0 & \alpha_{23}\mathcal{D}_- \\ 0 & 0 & \alpha_{23}^*\mathcal{D}_+ & 0 \end{bmatrix}. \quad (34)$$

With the ABAB stacking, we instead have

$$H_{ABAB} = \begin{bmatrix} 0 & \alpha_{01}\mathcal{D}_- & 0 & 0 \\ \alpha_{01}^*\mathcal{D}_+ & 0 & \alpha_{12}\mathcal{D}_+ & 0 \\ 0 & \alpha_{12}^*\mathcal{D}_- & 0 & \alpha_{23}\mathcal{D}_- \\ 0 & 0 & \alpha_{23}^*\mathcal{D}_+ & 0 \end{bmatrix}, \quad (35)$$

that is, with the chiralities of the matrix elements relating the second and third layers flipped. Thus, by restacking, it is possible to obtain several columns with only one chirality of Dirac operators and not both. Such columns will contribute with new zero-mode solutions and will increase the zero-mode degeneracy by a multiplicity factor. Assume that the flux is such that there are n solutions ψ_i ($i = 1, \dots, n$) to $\mathcal{D}_+\psi = 0$ and, hence, no solutions to $\mathcal{D}_-\psi = 0$. Then, there are only the n zero modes for H_{ABCA} in Eq. (34) of the form

$$\Psi = (\psi_i, 0, 0, 0)^T. \quad (36)$$

H_{ABAB} in Eq. (34), on the other hand, has the same n zero modes, but also n additional zero modes of the form

$$\Psi = (0, 0, \psi_i, 0)^T, \quad (37)$$

which are not solutions to H_{ABCA} because of the mixed occurrence of \mathcal{D}_+ and \mathcal{D}_- in the third column of H_{ABCA} . Thus, the Hamiltonian H_{ABCA} has twice as many zero modes. For a larger number of layers, one has an even bigger number of different stacking configurations to choose between, each with different implications for the zero-mode degeneracy. The one extreme case is given by the ‘‘face-centered-cubic’’ stacking ABCABC... (a configuration without flipped chiralities), which remains at the n zero modes for an arbitrary number of layers. The other extreme is given by the hexagonal close-packed stacking ABABAB... (with an alternating sequence of chiralities), where the number of zero modes of $2S + 1$ bands is $n(S + 1/2)$ for half-integer S , and nS or $n(S + 1)$ (depending on the sign of the flux) for integer S . Other stackings give some intermediate multiple of n zero modes. A quick inspection shows that the contribution from the other Dirac point just duplicates this result for any stacking configuration, thus there will be a factor of 2 due to valley degeneracy.

The above-observed flexibility to increase the zero-mode degeneracy by a simple change of stacking is in stark contrast with the situation in multilayer graphene. Multilayer graphene has, in the simplest approximations, indeed multiple times the degeneracy of the monolayer Hamiltonian.²⁸ However, although the structure of the Hamiltonian depends sensitively on the stacking,²⁹ the degeneracy turns out in the simplest approximation to be independent of stacking, even in the case of a nonuniform vector potential.³⁰

These results, in fact, also apply for magnetic fields that are no longer uniform. While, in this case, Landau-level degeneracies will in general be lifted, the $E = 0$ Landau level for $2d$ Dirac electrons is an exception. The reason is the widely known general property of Dirac operators in a vector potential

of arbitrary distribution, which is treated by the Atiyah-Singer index theorem,³¹ but can be understood also on a less formal level thanks to the neat argument by Aharonov and Casher.³² This may imply an $E = 0$ Landau level that is qualitatively sharper than the other Landau levels since only the latter are broadened by the nonuniform component of the magnetic field. In graphene, a nonuniform component can be due to the effective magnetic field introduced by the corrugation of the graphene membrane. That the $E = 0$ level remains relatively sharp in graphene has been observed in experiments.^{33,34} Even already for weak magnetic fields, one can expect an increased density of states at $E = 0$ due to these zero modes. If the degeneracy of the zero modes can be multiplied, as we have shown for our example, then such a peak in the density of states should grow with the same multiplicity.

Notice that the Landau-level degeneracy depends strongly on the chosen stacking of the layers, thus, also influencing the height of the zero-energy peak in the density of states. This is in stark contrast to the zero-field results, where the DOS is stacking independent, as studied in Sec. III.

VII. KLEIN TUNNELING ON A POTENTIAL STEP

Finally, we discuss Klein tunneling of spin- S Dirac electrons. As we have seen, qualitative differences arise between half-integer and integer spins. The transmission amplitude for spin-1/2 Dirac electrons has been studied, in connection to graphene, in Ref. 35. The spin-1 case and the influence of the flat band was studied in Refs. 3, 5, and 36, and all-angle perfect transmission was found at specific energies. Here, we discuss Klein tunneling for the pseudospin-1 case, and focus on tunneling into the flat band, as shown in Fig. 6.

But, before doing so, let us discuss the general matching conditions of the wave function for general pseudospin S . In this case, the spinor wave function takes the form (omitting spatial coordinates for simplicity)

$$\Psi = (\Psi_1, \Psi_2, \dots, \Psi_{2S}, \Psi_{2S+1})^T. \quad (38)$$

To determine the matching conditions,³⁶ we integrate the eigenvalue equation of the Hamiltonian in Eq. (6), or more

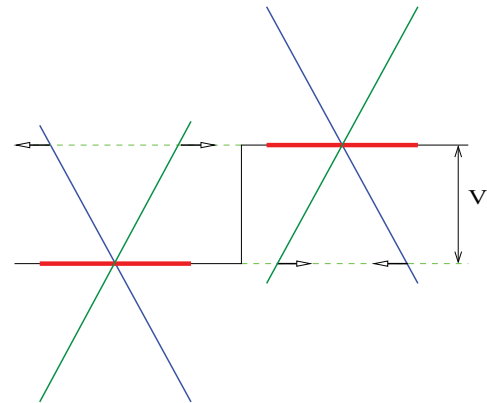


FIG. 6. (Color online) A sharp potential barrier for the spin-1 Dirac equation; the thick red lines denote the nonpropagating zero-energy states, while the short black arrows stand for the velocity of the branches.

generally from Eq. (4), after expanding it around the K point $H_S\Psi = E\Psi$ from $x = -x_0$ to x_0 and send x_0 to zero. As a result, we obtain, assuming nondiverging scalar and vector potentials,

$$\Psi_2(-x_0) = \Psi_2(x_0), \quad (39)$$

$$\begin{aligned} & \alpha_{i-1,i}^* \Psi_i(-x_0) + \alpha_{i,i+1} \Psi_{i+2}(-x_0) \\ & = \alpha_{i-1,i}^* \Psi_i(x_0) + \alpha_{i,i+1} \Psi_{i+2}(x_0) \text{ for } i = 1, \dots, 2S - 1, \end{aligned} \quad (40)$$

$$\Psi_{2S}(-x_0) = \Psi_{2S}(x_0). \quad (41)$$

In general, this implies that Ψ_2 and Ψ_{2S} must be continuous since there is only a single nonzero element in the first and last row of the Hamiltonian matrix. In addition, Eq. (40), involving other components of the spinor, contains only Ψ_i and Ψ_{i+2} , hence, there is no mixing between even and odd components.

The case of half-integer pseudospin (with even $2S + 1$) implies that the two continuous spinor components [Eqs. (39) and (41)] contain one even (2) and one odd ($2S$) index. Therefore, the continuity of, e.g., Ψ_2 implies through Eq. (40) that of Ψ_4 . The continuity of Ψ_4 in turn implies the continuity of Ψ_6 and so on. The very same procedure can be carried out for the odd components. Therefore, each component of the spinor changes continuously, thus, the whole wave function remains continuous across a potential barrier.

The case of integer pseudospins is different: $2S + 1$ is odd, therefore, only two even components (Ψ_2 and Ψ_{2S}) are required to change continuously (as opposed to the one even and one odd component for half-integer S). This implies that all even components must be continuous, but there are only S equations for the remaining $S + 1$ odd components. Only the continuity of the linear combinations of neighboring odd components [Eq. (40) with $i = 1, 3, \dots, 2S - 1$] is required across a barrier, but nothing can be said about the individual components.

Similar considerations apply along the y directions, in which case the wave function still changes continuously for half-integer S , while only the even components remain continuous for integer S . Implicitly, this difference can be traced back to the absence or presence of a flat band.

Here, we consider the scattering of pseudospin-1 electrons on a sharp potential step of the form $V\Theta(x)$, $V > 0$. The case when the energy of the injected electron differs from V has already been considered in Refs. 3 and 36. However, when the energy of the incident electron is exactly $E = V$, scattering into the nonpropagating flat band becomes possible. The electrons on the flat band do not possess a well-defined Fermi surface since all particles residing on the flat band have identically zero energy. Thus, an incident electron with $E = V$ can be scattered to any momentum state of the flat band within the barrier.

At normal incidence ($k_y = 0$), there is perfect transmission ($T = 1$) since transmission to the upper or lower Dirac cones is possible (excluding the flat band).

At a finite angle, scattering to the propagating cones is forbidden by momentum conservation (k_y does not change). In this special case, the wave function on the left- and right-hand side of the barrier [suppressing the $\exp(ik_y y)$ term] is

given by

$$\begin{aligned} \Psi^L(x < 0) = & \frac{1}{2} \begin{pmatrix} \exp(i\varphi_k) \\ \sqrt{2}\alpha \\ \exp(-i\varphi_k) \end{pmatrix} \exp(ik_x x) \\ & + \frac{r}{2} \begin{pmatrix} -\exp(-i\varphi_k) \\ \sqrt{2}\alpha \\ -\exp(i\varphi_k) \end{pmatrix} \exp(-ik_x x), \end{aligned} \quad (42)$$

$$\begin{aligned} \Psi^R(x > 0) = & \sum_{k'_x} \frac{t(k')}{\sqrt{2}} \begin{pmatrix} \exp(i\varphi_{k'}) \\ 0 \\ -\exp(-i\varphi_{k'}) \end{pmatrix} \exp(ik'_x x) \\ & + a \begin{pmatrix} \Theta(k_y) \\ 0 \\ \Theta(-k_y) \end{pmatrix} \exp(-|k_y|x), \end{aligned} \quad (43)$$

where k_y is conserved, i.e., $k_y = k'_y$, $V = v|k|$, $\tan(\varphi_k) = k_x/k_y$, $\tan(\varphi_{k'}) = k'_x/k_y$, and the lack of Fermi surface implies that any state on the flat band is available for transmission without any restrictions on k'_x , explaining the summation over k'_x , $\alpha = 1$. The last term describes an evanescent mode in the flat band. Applying the continuity of Ψ_2 from Eq. (39) implies that the reflection coefficient $r = -1$, from which the reflection probability is $R = |r|^2 = 1$, and $T = 0$.

As far as such a stationary solution is concerned, states in the flat band to the right of the barrier may also be occupied. However, as the group velocity on the flat band is zero, the transmission probability is also zero, or in other words, the probability current is zero through the barrier. The resulting picture thus consists of standing, nonpropagating waves, extending to both sides of the barrier: on the left, it is made of two counterpropagating waves (in the x direction), the interference of which leads to a standing wave, while on the right, the zero-energy mode is nonpropagating by its very nature. Although the wave function to the left of the barrier is uniquely determined by specifying energy $E = V$ and perpendicular momentum k_y , its corresponding part to the right of the barrier has many degenerate versions due to the flat band, and can thus host a large number of different states $\sim L$, even for a fixed k_y .

This can be made explicit as follows. By using Eq. (40) to connect Eqs. (42) and (43), we get

$$\cos(\varphi_k) = \frac{a}{2} + \frac{i}{\sqrt{2}} \sum_{k'_x} t(k') \sin(\varphi_{k'}), \quad (44)$$

which can have $\sim L$ distinct set of independent solutions in terms of $\{t(k')\}$ and a . Crucially, each such solution corresponds to zero transmission probability and perfect reflection. Very similar considerations apply to the case of $E = 0$, namely, an electron in the flat band to the left of the barrier, scattered to propagating states to the right.

In the presence of many bands ($S > 1$), tunneling between them occurs with a greater variety, and interband tunneling is also possible between propagating bands. However, the main difference is still expected from the presence or absence of a flat band (half-integer versus integer S), as is also reflected in the different matching conditions.

VIII. POSSIBLE EXPERIMENTS

In this section, we discuss the experimental possibilities to create optical lattices, which would realize the spin- S Dirac equation, and the methods to observe the characteristic physical quantities. This section gives a brief overview of which concrete protocols have been proposed in the cold-atom literature over the past few years; some of them are of course still under active development. Indeed, there is a significant and ongoing experimental effort devoted to realize lattices with exotic band structures (for recent examples on triangle-based lattices, see Refs. 37 and 38). Attempts to realize the family of lattices proposed here would form part of this endeavor.

As we have already mentioned, the lattice structure in Fig. 1 can be regarded as face-centered-cubic lattice, which in itself (being a Bravais lattice) is relatively straightforward to generate. As a first option, this can be created by four laser beams at the appropriate angle, realized and discussed in detail in Refs. 39–42. Although the triangular layers would be *a priori* equidistant, a setup like that of Ref. 39 already treats the lasers in one [111] direction inequivalently from the others, so that the relative strengths for intraplane and interplane hopping need not be equal. Making the former much weaker than the latter (even without adding further laser beams, relative angles and intensities of the beams are tunable) will then yield a band structure including the presence of the flat band, as described above. To achieve the chosen number layers, one can, e.g., create an optical superlattice in the perpendicular direction to the layers⁴³ or by utilizing blue-detuned light sheets to terminate the layered structure. Particles are then mainly confined to these triangular layers, the number of which defines $2S + 1$.

Second, one can profit from the versatility of a holographic mask, enabling arbitrary geometries, to generate the desired lattice structure.⁴⁴ Another option is to follow the steps outlined in Ref. 6 and to introduce spin-dependent hopping amplitudes, which in turn also realize the desired multiple Dirac-cone structure.

In terms of observables, the presence of the flat band can be revealed by time-of-flight imaging since particles residing on the flat band remain immobile⁵ and would show up as missing particles. In addition, the number of particles (the integral of the density of states) on the lattice as a function of the chemical potential could be monitored, which a jump around zero energy for integer S due to the large degeneracy of the flat band.² The particle number per lattice site and physical spin behaves close to half-filling as

$$N(\mu \simeq 0) - \frac{2S + 1}{2} = \frac{\delta_{S,\text{integer}} \text{sign}(\mu) + \rho(\mu)\mu}{2}, \quad (45)$$

where $\rho(\mu)$ is the DOS, which can be obtained by taking the numerical derivative of the experimentally measured particle number with respect to μ . The DOS can also conveniently be measured by rf spectroscopy, which directly probes the momentum-integrated spectral function, i.e., the DOS.⁴⁵ The momentum-resolved Raman spectroscopy can also be used for the same purpose.

The density-density correlation function, which is readily related to the optical conductivity,⁴⁵ can be investigated by shot noise measurement, while the optical conductivity can

directly be probed by the amplitude or phase modulation of the optical lattice.⁴⁶ Thanks to the modulation, the energy absorption rate or the doublon production rate turns out to be directly proportional to $\sigma(\omega)$.

To probe the spin-Hall effect, an effective electric field should be applied by tilting the lattice along one direction, and the detection of the spin-current accumulation through separate imaging of the two different spin components⁴⁷ could reveal the quantization of the spin-Hall conductivity, stemming from the underlying topology of the band structure.

Work in progress on realizing artificial gauge fields holds the promise to probe the Landau-level degeneracy. These gauge fields mimic the effect of a real vector potential, thus leading to the formation of Landau levels. The enhanced degeneracy of the zero-energy level should be revealed by time-of-flight imaging, as discussed above, or by rf spectroscopy. In addition, the Hall current can be made visible by driving the system out of equilibrium by suddenly changing the trapping potential and measuring the Hall current.⁴⁸

Additional methods for detecting topological properties, such as quantized Hall conductivity⁴⁹ and chiral edge states,⁵⁰ have been discussed recently in the literature and could be generalized to our lattice setup.

Klein tunneling is expected to be observed in the presence of smooth potential barrier, achievable by an accelerated optical lattice potential⁵¹ or by simply tilting the lattice.⁵² Both methods would give rise to an additional potential term, varying linearly in one direction as $V(\mathbf{r}) \sim x$. A sharp potential barrier is also available using the appropriate holographic masks. The characteristics of Klein tunneling (i.e., perfect transmission at given angles) should show up in the measured momentum distribution.

Finally, we mention in passing that photonic crystals allow the realization of the appropriate lattice geometry,⁵³ sketched in Fig. 1. The nature of the edge states can be probed similarly to Ref. 54, together with the characteristics of Klein tunneling.

IX. CONCLUSIONS

In conclusion, we have studied the lattice generalization of the spin-1/2 Dirac equation of graphene to arbitrary spin. The main difference arises between integer and half-integer spins, the former possessing a flat band, which is absent for graphene (corresponding to $S = 1/2$). As a result, the density of states and the optical conductivity are modified, and the topological properties are also enriched. We would like to reemphasize the following points.

First, even in the absence of a perfect $\mathbf{S} \cdot \mathbf{p}$ Hamiltonian, the above multicone picture can survive with a different ratio of the opening angles between the cones.

Second, a flat band is expected under general conditions in the gapless case: any lattice with an odd number of layers and with chiral symmetry is expected to have a flat band. In the gapped case, the flat band is less general, but can still be realized in some natural settings among the case of equidistant layers with regular stacking.

Third, some topological properties depend sensitively on the stacking configuration. We have established this for the Aharonov-Casher zero modes in a random magnetic field.

Also, the Chern numbers of individual bands are strongly stacking dependent.

Fourth, while the wave function remains continuous across a potential barrier for half-integer pseudospin, only its even components remain continuous for integer S .

Last, we would like to emphasize that the lattice structure in Fig. 1 simply corresponds to a four-layer slab of the face-centered-cubic Bravais lattice squeezed in the [111] direction.

ACKNOWLEDGMENTS

We thank J. Asbóth, H.-P. Buechler, J. Cserti, G. Kells, F. Simon, S. Sondhi, and A. Virosztek for stimulating discussions and comments, and D. Bercioux for pointing out an error in the previous version and for bringing Ref. 36 to our attention. Support by the Hungarian Scientific Research Funds No. K72613, No. K73361, and No. CNK80991 and New Széchenyi Plan No. TÁMOP-4.2.1/B-09/1/KMR-2010-0002, and by the Bolyai program of the Hungarian Academy of Sciences is acknowledged. B. D. was partially supported by ERC Grant No. ERC-259374-Sylo, J. K. is grateful for the hospitality of APCTP, South Korea.

APPENDIX: SYMMETRY CONDITIONS FOR FLAT BANDS

In this Appendix, we discuss in further detail the different symmetry properties both of the full Hamiltonian in Eq. (4) as well as of its low-energy expansion around the Dirac points of which the spin S Hamiltonian equation (6) is a special case. We will show that the existence of the flat band in the different settings can be understood in terms of symmetries, and that the symmetry conditions in the different settings are of different level of generality, that is, of different level of robustness to variations in the parameters of the model.

In the gapless case, the flat band is protected by a very general symmetry, the chiral symmetry, which is made possible by the bipartite nature of the lattice and is present under the considered nearest-neighbor hopping, which respects this bipartiteness (bipartiteness will be explained below). The flat band is insensitive to arbitrary variations of the parameters α_{ij} , for example, due to small misalignments of the lattice, as this does not change the bipartite structure of the Hamiltonian.

The situation is changed when one introduces any diagonal terms, for example, due to intralayer hopping or in the form of a gap term such as, for example, ΔS_z . Such terms do not respect the bipartite structure and lead to the violation of the chiral symmetry. However, less general symmetries protecting flat bands can still be at play. The flat band will no longer be robust to any small arbitrary variations in the parameters. However, it will still be there for a rather wide class of parameter configurations, including fortunately some rather natural configurations such as equidistant layers. We will now discuss these symmetry issues in further detail, starting with the chiral symmetry.

A lattice is bipartite if the sites can be collected into two partitions A and B and the Hamiltonian only contains nonzero matrix elements between the partitions, but not within each partition (which is the case of the nearest-neighbor hopping on the honeycomb lattice, which gives the free massless Dirac Hamiltonian). In our multilayer generalization, the partitions

are the odd and even layers, respectively. Chiral symmetry is present as the only terms in the Hamiltonian are the hoppings between adjacent layers. In contrast, hopping *within* the layers of triangular lattices would be one source of diagonal terms in the Hamiltonian equation (4). A transverse electric field would be another source. Such diagonal terms break the chiral symmetry.

We are now going to discuss on a more mathematical level the conjugation symmetry properties of the model Hamiltonian H_S

$$= t \begin{bmatrix} \Delta_0 & \alpha_{01} f(\mathbf{k}) & 0 & & \\ \alpha_{01}^* f^*(\mathbf{k}) & \Delta_1 & \alpha_{12} f(\mathbf{k}) & & 0 \\ 0 & \alpha_{12}^* f^*(\mathbf{k}) & 0 & \ddots & \\ & & 0 & \ddots & \alpha_{2S-1,2S} f(\mathbf{k}) \\ & & & 0 & \alpha_{2S-1,2S}^* f^*(\mathbf{k}) & \Delta_S \end{bmatrix}. \quad (\text{A1})$$

When the gap terms are zero $\Delta_i = 0$, the Hamiltonian possesses a chiral symmetry (CS): $\Sigma H(\mathbf{k}) \Sigma^\dagger = -H(\mathbf{k})$, where Σ is a unitary matrix. The CS conjugates the spectrum. In our case, we have $\Sigma = \text{diag}(1, -1, 1, -1, \dots)$ generalizing $\Sigma = \sigma_z$, which conjugates the gapless $S = \frac{1}{2}$ Dirac spectrum. In the case of an odd number of bands, the CS has to map the middle-most band onto itself. Furthermore, since the CS conjugates the spectrum at each \mathbf{k} separately, each (crystal) momentum eigenstate in the middle band has to map onto itself. Chiral symmetry guarantees thus a zero-energy state at each \mathbf{k} , i.e., a flat band. This should be contrasted with particle-hole symmetry (PHS) $U_{\text{PH}} H^*(\mathbf{k}) U_{\text{PH}}^\dagger = -H(-\mathbf{k})$, also possessed by the same Hamiltonian. PHS conjugates the band structure, however, it does not do so at each \mathbf{k} independently, wherefore PHS alone is not enough to guarantee a flat band.⁵⁵

The chiral symmetry is not only independent of the precise values of the parameters α_{ij} 's, but also of the stacking. As the chiral symmetry only relies on bipartiteness, it is also independent to changes in the stacking with the consequent individual flipping of chiralities in the tunneling between the involved layers, as for the Hamiltonian equation (10).

For the gapped case, the chiral symmetry is lost and there are no general symmetries to guarantee a flat band. Nonetheless, the following conditions are still sufficient for the appearance of a flat band in the general case with a nonzero gap. The diagonal gap term $\text{diag}(\Delta_0, \Delta_1, \dots, \Delta_{2S})$ must satisfy the antisymmetric property $\Delta_{2S} = -\Delta_0$, $\Delta_{2S-1} = -\Delta_1$, etc. At the same time, the off-diagonal elements with the α parameters must satisfy a symmetric property in their moduli: $|\alpha_{2S-1,S}| = |\alpha_{01}|$, $|\alpha_{2S-2,S-1}| = |\alpha_{12}|$, etc., while the phases can be chosen arbitrarily. For this reason, the flipping of chiralities between layers does not change anything since $|f^*| = |f|$.

Even though it is difficult to interpret these general conditions in terms of symmetries, these can be connected, in some special cases, to a symmetry property specific to the Dirac cone, that is, they are present only in the low-energy approximation for the system close to half-filling. For example, if one imposes the stronger condition $\alpha_{2S-1,S} = \alpha_{01}$, $\alpha_{2S-2,S-1} = \alpha_{12}$, \dots , and a symmetric configuration of flipped chiralities, then the flat bands can be seen as a consequence of the emergent conjugation property $Y H_S^*(\mathbf{p}) Y^\dagger = -H_S(\mathbf{p})$, with \mathbf{p} being the small momentum with respect to a Dirac

point and with Y generalizing σ_y as a matrix with the alternating pattern $(-i, i, -i, i, \dots)$ on the antidiagonal of the matrix (i.e., the diagonal joining bottom-left and top-right entries). It formally looks like a PH symmetry combined with inversion symmetry $H(-\mathbf{p}) = H(\mathbf{p})$, however, with momenta not inverted around $\mathbf{k} = 0$ as the physical PH symmetry requires, but around the Dirac point $\mathbf{p} = \mathbf{k} - \mathbf{k}_+ = 0$.

As mentioned in the beginning of the section, some of the specific parameter configurations are rather natural. For

equidistant layers, the gap parameter is ΔS_z and can be created by the electrostatic potential of a uniform transverse electric field. The α 's would all have the same modulus for equidistant layers and therefore also fulfill the above conditions, although they would not correspond to the values pertinent to S_x and S_y . Thus, we conclude that equidistant layers for certain symmetric stackings are enough to guarantee flat bands also in the presence of a gap term generated by a transverse uniform electric field.

*dora@pks.mpg.de

¹K. S. Novoselov, A. K. Geim, S. V. Morozov, D. Jiang, Y. Zhang, S. V. Dubonos, I. V. Grigorieva, and A. A. Firsov, *Science* **306**, 666 (2004).

²D. Bercioux, D. F. Urban, H. Grabert, and W. Hausler, *Phys. Rev. A* **80**, 063603 (2009).

³R. Shen, L. B. Shao, B. Wang, and D. Y. Xing, *Phys. Rev. B* **81**, 041410(R) (2010).

⁴D. Green, L. Santos, and C. Chamon, *Phys. Rev. B* **82**, 075104 (2010).

⁵V. Apaja, M. Hyrkäs, and M. Manninen, *Phys. Rev. A* **82**, 041402(R) (2010).

⁶Z. Lan, N. Goldman, A. Bermudez, W. Lu, and P. Öhberg, *Phys. Rev. B* **84**, 165115 (2011).

⁷M. P. Kennett, N. Komeilizadeh, K. Kaveh, and P. M. Smith, *Phys. Rev. A* **83**, 053636 (2011).

⁸A. H. Castro Neto, F. Guinea, N. M. R. Peres, K. S. Novoselov, and A. K. Geim, *Rev. Mod. Phys.* **81**, 109 (2009).

⁹M. Z. Hasan and C. L. Kane, *Rev. Mod. Phys.* **82**, 3045 (2010).

¹⁰This ties in with the observation of Ref. 4 that flat bands go along with integer-spin Berry's phases.

¹¹H. Watanabe, Y. Hatsugai, and H. Aoki, e-print [arXiv:1009.1959](https://arxiv.org/abs/1009.1959).

¹²<http://www.easyspin.org/>.

¹³T. T. Heikkilä, N. B. Kopnin, and G. E. Volovik, *Pis'ma Zh. Eksp. Teor. Fiz.* **94**, 252 (2011) [*JETP Lett.* **94**, 233 (2011)].

¹⁴L. Fritz, J. Schmalian, M. Müller, and S. Sachdev, *Phys. Rev. B* **78**, 085416 (2008).

¹⁵D. J. Thouless, M. Kohmoto, M. P. Nightingale, and M. den Nijs, *Phys. Rev. Lett.* **49**, 405 (1982).

¹⁶F. D. M. Haldane, *Phys. Rev. Lett.* **61**, 2015 (1988).

¹⁷K. Sun, Z. Gu, H. Katsura, and S. Das Sarma, *Phys. Rev. Lett.* **106**, 236803 (2011).

¹⁸T. Neupert, L. Santos, C. Chamon, and C. Mudry, *Phys. Rev. Lett.* **106**, 236804 (2011).

¹⁹E. Tang, J.-W. Mei, and X.-G. Wen, *Phys. Rev. Lett.* **106**, 236802 (2011).

²⁰C. L. Kane and E. J. Mele, *Phys. Rev. Lett.* **95**, 226801 (2005).

²¹G. W. Semenoff, *Phys. Rev. Lett.* **53**, 2449 (1984).

²²L. Fu and C. L. Kane, *Phys. Rev. B* **76**, 045302 (2007).

²³D. Bercioux, N. Goldman, and D. F. Urban, *Phys. Rev. A* **83**, 023609 (2011).

²⁴C. Weeks and M. Franz, *Phys. Rev. B* **82**, 085310 (2010).

²⁵E. McCann and V. I. Fal'ko, *Phys. Rev. Lett.* **96**, 086805 (2006).

²⁶K. Novoselov, E. McCann, S. Morozov, V. Fal'ko, M. Katsnelson, U. Zeitler, D. Jiang, F. Schedin, and A. Geim, *Nat. Phys.* **2**, 177 (2006).

²⁷M. O. Goerbig, e-print [arXiv:1004.3396](https://arxiv.org/abs/1004.3396).

²⁸E. McCann and V. I. Fal'ko, *Phys. Rev. Lett.* **96**, 086805 (2006).

²⁹H. Min and A. H. MacDonald, *Phys. Rev. B* **77**, 155416 (2008).

³⁰J. Kailasvuori, *Europhys. Lett.* **87**, 47008 (2009).

³¹M. Nakahara, *Geometry Topology and Physics* (IOP Publishing, Bristol, 1999).

³²Y. Aharonov and A. Casher, *Phys. Rev. A* **19**, 2461 (1979).

³³A. J. M. Giesbers, U. Zeitler, M. I. Katsnelson, L. A. Ponomarenko, T. M. Mohiuddin, and J. C. Maan, *Phys. Rev. Lett.* **99**, 206803 (2007).

³⁴J. Martin, B. E. Feldman, R. T. Weitz, M. T. Allen, and A. Yacoby, *Phys. Rev. Lett.* **105**, 256806 (2010).

³⁵M. I. Katsnelson, K. S. Novoselov, and A. K. Geim, *Nat. Phys.* **2**, 620 (2006).

³⁶D. F. Urban, D. Bercioux, M. Wimmer, and W. Häusler, *Phys. Rev. B* **84**, 115136 (2011).

³⁷G.-B. Jo, J. Guzman, C. K. Thomas, P. Hosur, A. Vishwanath, and D. M. Stamper-Kurn, e-print [arXiv:1109.1591](https://arxiv.org/abs/1109.1591).

³⁸J. Struck, C. Ölschläger, R. L. Targat, P. Soltan-Panahi, A. Eckardt, M. Lewenstein, P. Windpassinger, and K. Sengstock, *Science* **333**, 996 (2011).

³⁹G. Grynberg, B. Lounis, P. Verkerk, J.-Y. Courtois, and C. Salomon, *Phys. Rev. Lett.* **70**, 2249 (1993).

⁴⁰K. I. Petsas, A. B. Coates, and G. Grynberg, *Phys. Rev. A* **50**, 5173 (1994).

⁴¹C. S. Adams, S. G. Cox, E. Riis, and A. S. Arnold, *J. Phys. B: At., Mol. Opt. Phys.* **36**, 1933 (2003).

⁴²D. Mei, B. Cheng, W. Hu, Z. Li, and D. Zhang, *Opt. Lett.* **20**, 429 (1995).

⁴³L. Guidoni and P. Verkerk, *J. Opt. B: Quantum Semiclassical Opt.* **1**, R23 (1999).

⁴⁴W. S. Bakr, J. I. Gillen, A. Peng, S. Fölling, and M. Greiner, *Nature (London)* **462**, 74 (2009).

⁴⁵G. D. Mahan, *Many Particle Physics* (Plenum, New York, 1990).

⁴⁶A. Tokuno and T. Giamarchi, *Phys. Rev. Lett.* **106**, 205301 (2011).

⁴⁷S.-L. Zhu, H. Fu, C.-J. Wu, S.-C. Zhang, and L.-M. Duan, *Phys. Rev. Lett.* **97**, 240401 (2006).

⁴⁸R. N. Palmer, A. Klein, and D. Jaksch, *Phys. Rev. A* **78**, 013609 (2008).

⁴⁹R. O. Umucalilar, H. Zhai, and M. O. Oktel, *Phys. Rev. Lett.* **100**, 070402 (2008).

⁵⁰N. Goldman, I. Satija, P. Nikolic, A. Bermudez, M. A. Martin-Delgado, M. Lewenstein, and I. B. Spielman, *Phys. Rev. Lett.* **105**, 255302 (2010).

⁵¹M. Ben Dahan, E. Peik, J. Reichel, Y. Castin, and C. Salomon, *Phys. Rev. Lett.* **76**, 4508 (1996).

⁵²M. Raizen, C. Salomon, and Q. Niu, *Phys. Today* **50(7)**, 30 (1997).

⁵³M. J. Escuti and G. P. Crawford, *Opt. Eng.* (Bellingham, WA, US) **43**, 1973 (2004).

⁵⁴Z. Wang, Y. Chong, J. D. Joannopoulos, and M. Soljacic, *Nature (London)* **461**, 772 (2009).

⁵⁵One could imagine a single band $\sim \sin k_x + \sin k_y$. It is not flat, but has the self-conjugate property upon $\mathbf{k} \rightarrow -\mathbf{k}$.